Lab on a Chip

PAPER

View Article Online
View Journal | View Issue

Check for updates

Cite this: *Lab Chip*, 2017, **17**, 1625

Multi-chamber microfluidic platform for high-precision skin permeation testing

M. Alberti, †[a] Y. Dancik, †*[bc] G. Sriram, [b] B. Wu,[a] Y. L. Teo,[c] Z. Feng,[a] M. Bigliardi-Qi,[bc] R. G. Wu,[a] Z. P. Wang‡*[a] and P. L. Bigliardi‡[bc]

The established *in vitro* tool used for testing the absorption and penetration of chemicals through skin in pharmacology, toxicology and cosmetic science is the static Franz diffusion cell. While widespread, Franz cells are relatively costly, low-throughput and results may suffer from poor reproducibility. Microfluidics has the potential to overcome these drawbacks. In this paper, we present a novel microfluidic skin permeation platform and validate it rigorously against the Franz cell by comparing the transport of 3 model chemicals of varying lipophilicity: caffeine, salicylic acid and testosterone. Permeation experiments through silicone membranes show that the chip yields higher sensitivity in permeant cumulative amounts and comparable or lower coefficients of variation. Using a skin organotypic culture, we show that the chip decreases the effect of unstirred water layers that can occur in static Franz cells. The validation reported herein sets the stage for efficient skin permeation and toxicity screening and further development of microfluidic skin-on-chip devices.

Received 23rd December 2016,
Accepted 3rd April 2017

DOI: 10.1039/c6lc01574c

rsc.li/loc

Open Access Article. Published on 03 April 2017. Downloaded on 9/22/2024 3:56:12 AM.
This article is licensed under a Creative Commons Attribution 3.0 Unported Licence.

Introduction

High-throughput, reliable and cost-effective *in vitro* skin permeation assays are in high demand. In pharmaceutical science, transdermal drug delivery (TDD) is a major area of research and development due to the advantages of cutaneous over oral drug administration for certain classes of compounds. This includes drugs requiring a prolonged period of delivery, high potency drugs with a short biological half-life and those subject to a significant hepatic first-pass effect.[1] The sheer number of possible drug/vehicle interactions necessitates fast and effective screening methods for drug formulation design.[2] In toxicology and risk assessment, estimating toxicity following skin exposure of consumer products, pesticides or lipophilic industrial solvents is of major concern.[3–5] With the European Union's 2007 Registration, Evaluation, Authorization and Restriction of Chemicals (REACH) regulation having drastically increased the number of chemicals that need to be evaluated for toxicity[6] and the European Union's 2013 ban on the use of animals in cosmetic product testing,

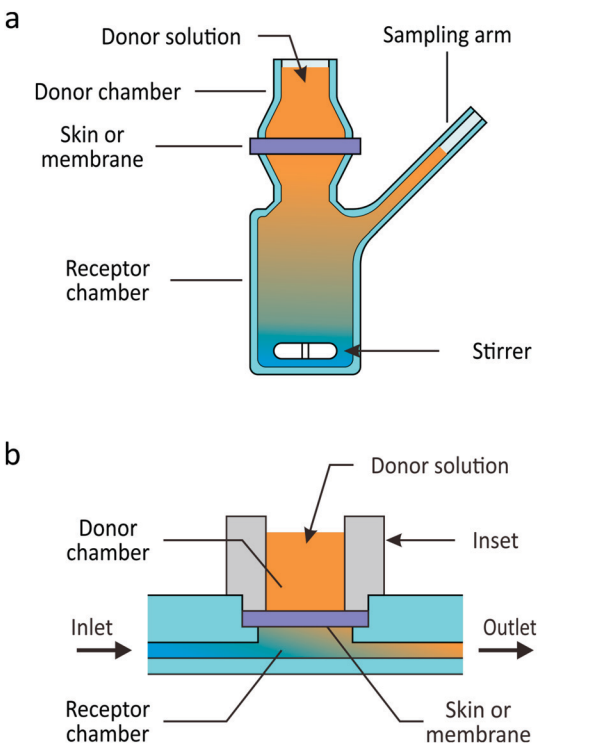

Fig. 1 Schematic illustrations of (a) the static Franz diffusion cell and (b) a permeation unit of the microfluidic permeation array (μFPA). In the μFPA, skin or a synthetic membrane is placed in the permeation chamber, and its edges sealed by an inset defining the diffusion area. The receptor chamber is provided with inlet and outlet channels, and it is perfused with a receiver solution into which the compound of interest permeates.

[a] *Singapore Institute of Manufacturing Technology, A*STAR, 2 Fusionopolis Way, Level 10, Innovis, 138634 Singapore. E-mail: yuri.dancik@imb.a-star.edu.sg, zpwang@simtech.a-star.edu.sg*
[b] *Experimental Dermatology Laboratory, Institute of Medical Biology, A*STAR, 8a Biomedical Grove, #06-06, 138648 Singapore*
[c] *Clinical Research Unit for Skin, Allergy and Regeneration, Institute of Medical Biology, A*STAR, 8a Biomedical Grove, #06-06, 138648 Singapore*
† These authors contributed equally to this work.
‡ Equal contribution as supervising authors.

Open Access Article. Published on 03 April 2017. Downloaded on 9/22/2024 3:56:12 AM.
This article is licensed under a Creative Commons Attribution 3.0 Unported Licence.

toxicology and cosmetic science have a similar need for the development and validation of high-throughput, alternative skin permeation testing methods.

The traditional systems for *in vitro* skin permeation testing are the static Franz and flow-through diffusion cells, in which excised skin or a skin substitute is sandwiched between a donor compartment and a receptor compartment (Fig. 1a). Sampling of the receptor solution occurs at predetermined times following application of a donor solution. This yields profiles of the concentration or cumulative amount over time of the compound of interest, from which transport parameters can be derived. Though widely used, Franz cells' typical diffusion areas of 1 to 3 cm^2, receptor volumes on the order of a few mL and time-consuming procedures render them relatively costly and low-throughput.[7] In addition, an unstirred water layer (UWL) may form in the static Franz cell when highly permeable membranes and lipophilic chemicals are used. Supplementary experiments and calculation are necessary to assess the effect of the UWL on the chemical's permeability through the membrane.[8,9]

Microfluidics has the potential to increase throughput and improve reproducibility of experimental skin simulations by providing cost-effective platforms that mimic the cutaneous physiological environment.[10] Microfluidic systems have been designed to grow a keratinocyte and dendritic cells coculture,[11] integrate *in vitro* skin models, cultures or biopsies and hair follicle units[12] or other tissues,[13,14] and to simulate and test perspiration.[15–17] Systems focusing on skin permeation include Mah *et al.*'s flow-through cell with rat or pig skin,[18] Abaci *et al.*'s pumpless microfluidic platform housing a human skin equivalent[19] and Provin *et al.*'s microfluidic diffusion cell with a lipid-coated polycarbonate membrane as a skin substitute.[20] Each of these permeability devices, however, was made of polydimethylsiloxane (PDMS), a material unsuitable for industrial mass production, incompatible with organic solvents and known to exhibit significant adsorption of small hydrophobic compounds.[21–24] Differences in design parameters between static and flow-through cell designs can contribute to variability in the final results.[8,25–28] Hence, there is a clear need for rigorous validation of novel microfluidic devices for skin permeation against the conventional systems. Given the growing number of organ-on-a-chip systems, such validation is also an important, often underestimated step towards the development of reliable skin-on-chips for *in vitro* permeation studies.

We present a novel microfluidic platform enabling high-throughput skin permeation testing in a flow-through design at a fraction of the material cost of Franz diffusion cells (Fig. 1b). This microfluidic permeation array (μFPA) is made of thermoplastic material, suitable for mass production. Synthetic membranes, excised animal or human skin, and skin organotypic cultures (skin-OTCs) can be easily integrated. The device's current design allows for six permeation experiments to be conducted simultaneously, important for reproducibility. The flow rate can be tuned to guarantee minimal permeant concentration in the receptor compartment in order to mimic the *in vivo* sink condition due to cutaneous blood flow.[29] We validated the μFPA against static Franz cells by comparing the steady-state permeation of caffeine, salicylic acid and testosterone. These chemicals cover a range of lipophilicities as recommended by the OECD guideline 428.[30,31] In a first instance, silicone membranes were used to avoid variability associated with skin. These experiments show that the μFPA yields lower limits of detection as well as lower coefficients of variation than the Franz cells. The μFPA was further tested for permeation through full-thickness skin-OTCs developed in-house. This latter experiment shows that the μFPA lessens the effect of unstirred water layers, a potentially significant pitfall of static Franz cells.[8]

Materials and methods

μFPA design and fabrication

The μFPA is composed of a multi-chamber microfluidic chip and a set of self-locking hollow cylindrical insets that define six independent permeation units symmetrically arranged in a 50 mm × 75 mm format (Fig. 2a). Six synthetic membrane disks or circular skin punches (7 mm in diameter) can be accommodated in the open chambers of the microfluidic chip. The edges of the membranes or skin pieces are sealed by the self-locking insets, if necessary equipped with elastomeric annuli. Each inset defines the donor chamber and the diffusion area of the permeation unit. The assembled device is a 6-chamber μFPA with diffusion areas of 0.2 cm^2, donor capacities of up to 300 μL and receptor volumes of 28 μL.

As shown in Fig. 2b, each microfluidic permeation unit is composed of a cylindrical permeation chamber; a locking station for the inset; a set of inlet and outlet channels; a debubbling unit integrated along the inlet channel; and embedded connectors. The receptor's inlet and outlet channels are 0.5 mm and 1 mm wide, respectively; all channels are 0.3 mm high. The inlet port is located in the upper surface of the chip in order to connect the inlet channel to the inlet tubing. The outlet port is located in the lower surface of the chip so that the rim of the embedded connector protrude out from the chip surface: this feature allows the outflow to drip directly into the collecting well without touching the chip surface, thus avoiding the spreading of the drops on the chip lower surface and compromising the collection volumes. The six outlet ports are regularly spaced as the wells of a 96-well plate.

The microfluidic chips were fabricated by thermally bonding together three microstructured thermoplastics layers, six circular polytetrafluoroethylene (PTFE) filter membranes (Fluoropore™, Merck KGaA, Germany), and twelve silicone rubber connectors (Fig. 2c).

All the chips used for permeation tests on silicone membranes were made of polycarbonate (PC). One chip made of PC and one made of poly(methyl methacrylate) (PMMA) were used for the permeation tests on skin-OTCs to check for variability due to the material. The microfluidic features were

 This journal is © The Royal Society of Chemistry 2017

Open Access Article. Published on 03 April 2017. Downloaded on 9/22/2024 3:56:12 AM.
This article is licensed under a Creative Commons Attribution 3.0 Unported Licence.

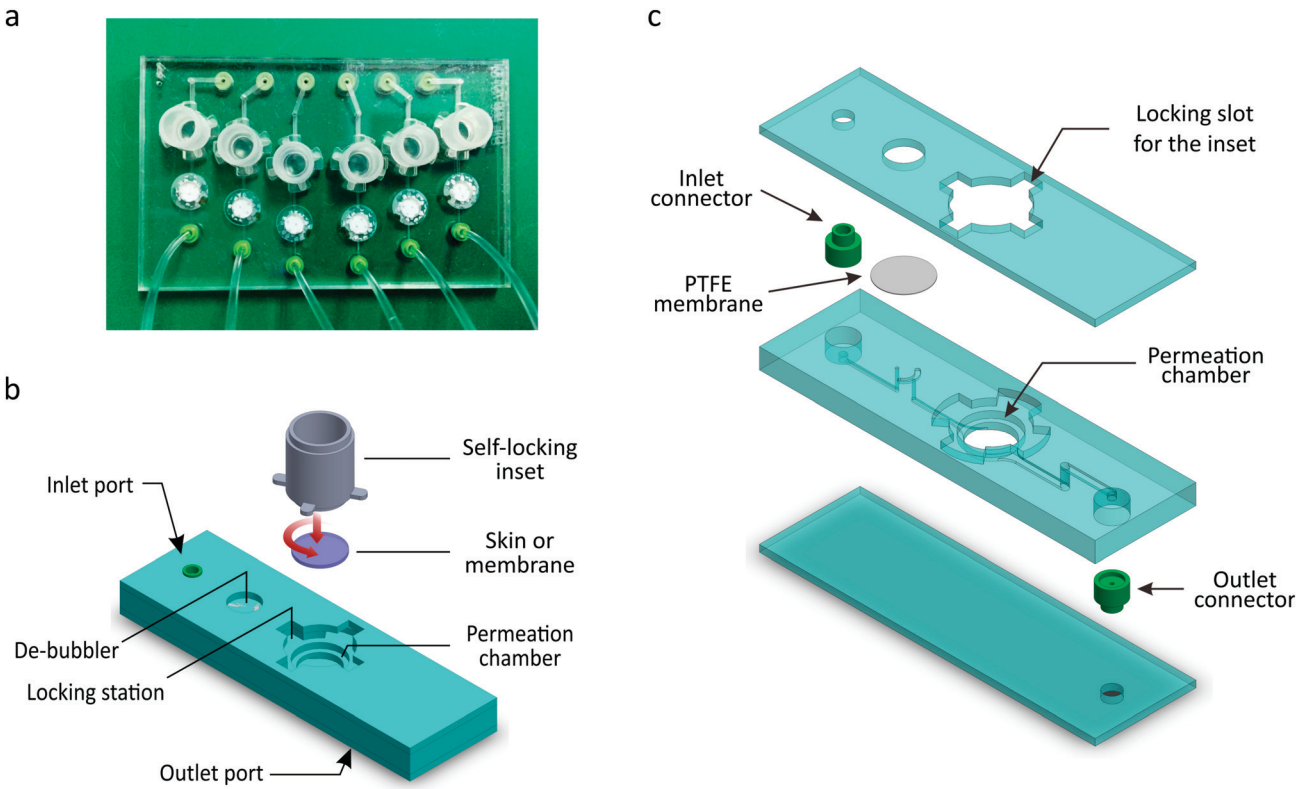

Fig. 2 (a) Top view image of the 6-chamber μFPA. (b) 3D illustration of a single permeation unit composing the μFPA and of the self-locking inset mechanism. The inset enables the sealing of the skin tissue or membrane into the permeation chamber. (c) Exploded view of the permeation microfluidic unit composing the chip.

microstructured in the polymer layers by micromilling. The PTFE filter membranes (8 mm in diameter) were placed between the second and the third layers, aligned with the microstructured features of the de-bubbling unit. The de-bubblers prevent bubbles from reaching the receptor chambers and affecting permeation. The tubing connectors were cast in silicone rubber (XIAMETER® RTV-4130-J, Dow Corning, USA) from a micromilled PMMA mould. The de-bubblers and connectors were fabricated according to designs and processes developed by SIMTech Microfluidic Foundry.[32]

The self-locking insets were fabricated in PC by micromilling. The inset has a hollow cylindrical body and four thin teeth (0.6 mm thick, 1.6 mm wide) protruding 1.8 mm from its lateral surface, perpendicularly to the cylinder axis (Fig. 2a). The locking station on the chip is composed of four docking slots arranged in a geometry corresponding to the inset's teeth. Each slot is composed of a vertical entrance for the tooth and a lateral (1 mm high) locking chamber.

The base of the inset is meant to clamp and seal the edges of the membrane or the skin tissue to avoid undesired flow of the donor solution through eventual gaps between the membrane and the walls of the diffusion chamber. When using skin-OTCs, a gasket annulus made of silicone (HT-6240 BISCO® transparent, Rogers Corporation, USA) is placed between the inset and the skin tissue in order to guarantee an adequate sealing. The inset may also allow placing a protective material on the membrane or skin and studying its influence on the permeation results.

Working principle

Once the membrane (or the skin tissue and a gasket annulus) is placed in the permeation chamber, the inset is mounted in the locking structure of the chip by aligning its teeth with the corresponding vertical entrances in the locking station, pressing it down and turning it counterclockwise to position and maintain the teeth inside the lateral slots (Fig. 2b). Once in the locking position, the inset compresses the edges of the membrane. This compression seals the system and at the same time generates a counterforce from the inset's teeth against the upper surface of the locking chambers that keeps the inset in place.

The inlets are connected to six 2-stop SC0002 Tygon® ST R-3607 tubings (Cole-Parmer GmbH, Germany) of an Ismatec® IPCN-12 peristaltic pump (Cole-Parmer GmbH, Germany) to supply the receptor buffer to each diffusion unit. The μFPA is positioned above a UV transparent 96-well plate so that each outlet port aligns with one row of microplate wells. The outflow is collected directly in the wells and, at the end of each time interval, the μFPA is slid above the plate until the outlet ports align to the wells of the next row (Fig. 3).

The pump flow rate and collection time intervals are tuned so that, unlike conventional flow-through systems, the

Open Access Article. Published on 03 April 2017. Downloaded on 9/22/2024 3:56:12 AM.
This article is licensed under a Creative Commons Attribution 3.0 Unported Licence.

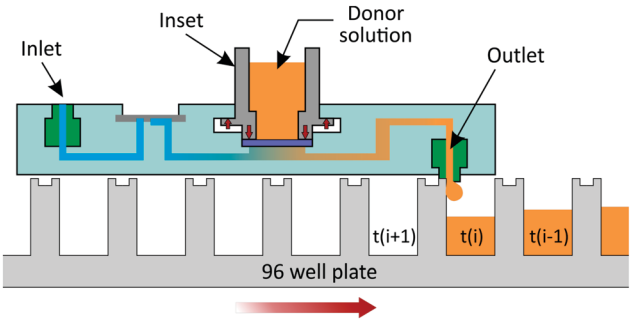

Fig. 3 Schematic illustration of the μFPA's working principle. The μFPA is placed on a 96-well plate such that the 6 outlet connectors are aligned with 6 wells of a given row. At the end of each time interval, the plate is moved until the outlet ports align with the next row of wells. The receptor solution is collected in each well from time $t(i-1)$ to $t(i)$. As the outlet connector protrudes slightly from the chip's bottom surface, contact between the connector and the edge of the well at time $t(i)$, when the plates is moved, prevents undesired spillage of the perfusate outside of the well.

entire perfusate is fractioned and collected directly in 96-well plates and easily assayed for concentrations.

Skin organotypic cultures

Immortalized human N/TERT-1 keratinocytes[33] were maintained in keratinocyte serum free medium (K-SFM, Gibco, ThermoFisher Scientific) supplemented with 0.09 mM calcium, 0.2 ng mL^{-1} epidermal growth factor (EGF, Gibco, ThermoFisher Scientific), 25 μg mL^{-1} bovine pituitary extract (Gibco, ThermoFisher Scientific) and 1% penicillin–streptomycin (PAN Biotech GmbH). Human primary foreskin-derived dermal fibroblasts were maintained in Dulbecco's modified Eagle medium (DMEM) supplemented with 10% fetal bovine serum and 1% penicillin–streptomycin.

Full-thickness skin-OTCs were fabricated using a fibrin-based dermal matrix as previously described by Toh *et al.*[34] Briefly, dermal equivalents were generated by encapsulating human dermal fibroblasts (2.5×10^5 cells per mL of matrix) within a fibrin-based matrix in a 6-well Falcon® cell culture insert (polyethylene terephthalate (PET) membrane, pore size 1 μm, Corning Life Sciences, MA, USA). The dermal equivalents were cultured in serum-free OTC medium-A comprising of Opti-MEM (Gibco, ThermoFisher Scientific), supplemented with 0.1% bovine serum albumin (BSA), hydrocortisone (50 μg mL^{-1}), ascorbic acid (10 mg mL^{-1}), 1% SITE supplement containing selenium (5 ng mL^{-1}), insulin (10 μg mL^{-1}), transferrin (5.5 μg mL^{-1}), and ethanolamine (2 μg mL^{-1}), 200 KIU mL^{-1} aprotinin (MP Biomedicals, CA, USA) and 1% penicillin/streptomycin. After 4 days, N/TERT-1 keratinocytes (4×10^5 cm^{-2}) were seeded on top of fibroblast-populated dermal equivalents and cultured under submerged conditions using serum-free OTC medium-B comprising of K-SFM supplemented with 0.1% BSA, hydrocortisone (50 μg mL^{-1}), ascorbic acid (10 mg mL^{-1}), 1% SITE supplement, 0.2 ng mL^{-1} EGF, 200 KIU mL^{-1} aprotinin, 1.2 mM calcium chloride and 1% penicillin/streptomycin. After 2 days, the organotypic cultures were moved to deep-well plates (Corning Life Sciences, MA, USA) and cultured at air–liquid interface for 2 weeks to allow differentiation, stratification, and cornification. During the air–liquid interface culture, serum-free OTC media-C comprised of K-SFM supplemented with 0.1% BSA, hydrocortisone (50 μg mL^{-1}), ascorbic acid (10 mg mL^{-1}), 1% SITE+3 supplement containing selenium (5 ng mL^{-1}), insulin (10 μg mL^{-1}), transferrin (5.5 μg mL^{-1}), ethanolamine (2 μg mL^{-1}), linoleic acid (4.7 μg mL^{-1}) and oleic acid (4.7 μg mL^{-1}), 200 KIU mL^{-1} aprotinin, 1.2 mM calcium chloride (MP Biomedicals, CA, USA) and 1% penicillin/streptomycin. All the media supplements were obtained from Sigma-Aldrich, unless otherwise specified.

Chemicals

Caffeine, salicylic acid, testosterone, isopropyl myristate (IPM), propylene glycol (PG) were obtained from Sigma-Aldrich, Singapore; ethanol (EtOH) from Merck KGaA (Germany), Dulbecco's phosphate buffered saline (PBS) from GE healthcare Life Sciences (USA). Solvents and concentrations (Table 1) were selected to obtain solutions corresponding to ~90% saturation, ensuring infinite applied doses and the onset of steady-state transport while allowing for mass balances to be measured.[35]

Silicone membrane and organotypic skin preparation

Prior to the permeation experiments, 2×2 cm^2 pieces of 0.05 cm-thick silicone membrane (HT-6240 BISCO® transparent, Rogers Corporation, USA) were equilibrated overnight in IPM for the caffeine and testosterone experiments, and in PBS for the salicylic acid experiments. The skin-OTCs attached to their support membranes were carefully cut out from the cell culture inserts using a scalpel on the day of the permeation experiment. Thicknesses of the silicone membrane and skin-OTCs pieces were measured using a digital caliper. Penetration experiments were also run on the PET membranes of the cell culture inserts to account for any diffusive resistance of the support membrane. For each compound, permeation experiments in the μFPA and in the Franz cells were conducted on the same day under the same environmental conditions.

Permeation experiments

μFPA. The permeation experiments with silicone membranes were conducted using PC chips. Disks of 7 mm in diameter were punched out of the pre-equilibrated silicone membrane pieces and clamped into the μFPA's permeation chambers.

The skin-OTCs experiment was performed with two different chips, one made of PC, the other of PMMA. In this way, the effect of material on inter-chip variability was assessed. Six circular pieces of skin-OTCs (7 mm in diameter) attached to support membranes were punched out of two cell culture inserts and integrated into the μFPAs such that each chip contained skin-OTCs from each insert. Six PC support membrane disks alone were inserted into the remaining

 This journal is © The Royal Society of Chemistry 2017

Open Access Article. Published on 03 April 2017. Downloaded on 9/22/2024 3:56:12 AM.
This article is licensed under a Creative Commons Attribution 3.0 Unported Licence.

Table 1 Experimental conditions for the permeation tests on silicone membranes

Permeant	Donor concentration 10^3 [μg mL^{-1}]	Vehicle	Membrane treatment	Receptor solution
Caffeine	13.5	PBS	IPM	PBS
Salicylic acid	2.92	PG : PBS (20 : 80)	PBS	PBS
Testosterone	7.07	EtOH : PBS (50 : 50)	IPM	EtOH : PBS (50 : 50)

permeation chambers. In each experiment, 275 μL of donor solution was applied to the silicone membrane or skin. To minimize evaporation during the experiments, the top openings of the self-locking insets (Fig. 3) were occluded with sealing tape (Petri-Seal™, Diversified Biotech, USA). Immediately after each experiment, the solutions remaining in the donor and in the receptor were collected for the mass balance. The receptor compartment was emptied by occluding the de-bubbler with sealing tape and infusing air into it. The sealing tape, the silicone membranes or skin pieces, the silicone annulus used in the skin experiments as well as the PBS used to wash the μFPA components were assayed.

Franz cells. Static Franz cells (PermeGear Inc., USA) with 0.64 cm^2 diffusion areas and 5 mL receptor volumes were used. In each experiment, 900 μL of donor solution was applied to the silicone membrane or skin, thus ensuring the same dose per cm^2 as in the μFPA. The receptor solution was continuously stirred with magnetic stirrers. To minimize evaporation, the donor compartment was occluded with parafilm. At each time point, a 200 μL sample was collected from the receptor compartment, which was then topped up with 200 μL of fresh receptor solution. Following each experiment, the donor solution and silicone membranes or skin pieces were collected, and the parafilm and all Franz cell components were washed with PBS for a mass balance.

Unstirred water layers. To interpret the difference in the skin-OTC permeation experiment with caffeine, additional experiments were conducted on both the μFPA and on Franz cells to check for the effect of an unstirred water layer (UWL). Based on Miller and Kasting's protocol,[8] the permeation of the same caffeine solution through 1, 2, and 3 dialysis membranes (Bel-Art Products, USA) mounted in series on Franz cells was assessed. Because it was not possible to accommodate and properly clamp 3 dialysis membranes in the μFPA diffusion chamber, the caffeine permeation through only 1 and 2 dialysis membranes was assessed on the microfluidic chip. The dialysis membranes have a molecular weight cut-off of 6000 Da and a thickness of 0.073 mm.

Analytical method

Concentrations were determined by UV spectroscopy using a microplate reader (Synergy™ H1, BioTek Instruments Inc., VT, USA). Caffeine, salicylic acid and testosterone peak absorbance readings were at 272 nm, 296 nm and 245 nm, respectively.

Data analysis

Transport model. Fick's second law of diffusion relates the permeant concentration in the membrane (silicone membrane or OTC skin), c_m, to depth x in the membrane, over time,

$$\frac{\partial c_m}{\partial t} = D_m \frac{\partial^2 c_m}{\partial x^2} \quad (1)$$

where D_m is the permeant diffusion coefficient in the membrane. The initial condition expressing a lack of permeant in the membrane and boundary conditions expressing a constant donor concentration in equilibrium with the membrane concentration and receptor sink conditions are:

$$\begin{aligned} &\text{Initial condition:} && c_m(x, t=0) = 0 \\ &\text{Boundary conditions:} && c_m(x=0, t) = K_{m/d} c_d \\ & && c_m(x=h_m, t) = 0 \end{aligned} \quad (2)$$

The solution to eqn (1) and (2) is often expressed as the cumulative amount of permeant in the receptor, $Q(t)$:

$$Q(t) = K_{m/d} c_d h_m A \left[\frac{D_m t}{h_m^2} - \frac{1}{6} - \frac{2}{\pi^2} \sum_{n=1}^{\infty} \frac{(-1)^n}{n^2} e^{\left(-\frac{D_m n^2 \pi^2 t}{h_m^2}\right)} \right] \quad (3)$$

In eqn (3), h_m designates the membrane thickness, $K_{m/d}$ the membrane/donor equilibrium partition coefficient and A the diffusion area. At steady state, the cumulative amount is given by

$$Q_{ss}(t) = K_{m/d} c_d h_m A \left[\frac{D_m t}{h_m^2} - \frac{1}{6} \right] \quad (4)$$

or, in terms of the steady state permeability coefficient (k_p), flux ($J_{ss} = k_p c_d$) and the lag time to steady-state (t_{lag}),

$$Q_{ss}(t) = k_p c_d A (t - t_{lag}) = J_{ss} A (t - t_{lag}) \quad (5)$$

The receptor solution concentrations obtained from the Franz cell and μFPA permeation experiments were converted to cumulative amounts. In the case of the μFPA results, this conversion accounts for the receptor flow rate. Regression of eqn (5) against the linear part of the experimental $Q_{ss}(t)$ profiles yields k_p, t_{lag} and J_{ss}.

The steady state 1D model can be extended to incorporate unstirred water layers (UWLs) above and below the membrane by considering the membrane and UWL steady state

Open Access Article. Published on 03 April 2017. Downloaded on 9/22/2024 3:56:12 AM.
This article is licensed under a Creative Commons Attribution 3.0 Unported Licence.

permeability coefficients as inverses of serial diffusive resistances. The total diffusive resistance is thus the sum of the resistances due to the membrane and the UWLs:

$$R_{total} = R_m + R_{uwl} \quad (6)$$

In the UWL experiments, linear regression of R_{total} against resistances from i dialysis membranes is conducted to obtain R_{uwl} according to eqn (7):[8]

$$R_{total} = iR_{dialysis\ m} + R_{uwl} \quad (7)$$

The total UWL thickness h_{uwl} is estimated from R_{uwl} and the diffusivity of the permeant of interest in dilute aqueous solution, D_w^∞:

$$h_{uwl} = D_w^\infty R_{uwl} \quad (8)$$

To estimate D_w^∞, the Wilke–Chang correlation[36] is used,

$$D_w^\infty = 7.4 \times 10^{-8} \frac{T\sqrt{\phi_w MW_w}}{\eta_w V_p^{0.6}} \quad (9)$$

where T is the temperature in Kelvin, $\phi_w = 2.6$ is the water association factor, MW_w is the solvent molecular weight, η_w = 0.89 cP is water viscosity at 25 °C and V_p is the permeant's molecular volume estimated from Schroeder's group contribution method.[37]

Numerical simulation

In the μFPA, permeant accumulation in the receptor chamber may be expected. It is described by the left-hand term of the general mass balance equation for flow-through diffusion cells:[26,28,38]

$$V_{rec}\frac{dC_{rec}}{dt} = JA - F_{rec}c_{rec} \quad (10)$$

where V_{rec} is the receptor chamber volume, c_{rec} the permeant concentration in the receptor chamber, J the permeant flux from the membrane into the receptor chamber, A the diffusion area and F_{rec} the receptor solution flow rate.

To evaluate the relevance of the accumulation for the three compounds, a finite element analysis of the 3D transport in the μFPA was implemented in COMSOL Multiphysics® (COMSOL Inc., USA). The membrane diffusion and partition coefficients (D_m, $K_{m/d}$) were estimated from the Franz cells experiments.

Caffeine and salicylic acid diffusivities in the receptor solution (PBS) were estimated using the Wilke–Chang correlation[36] (eqn (9)). Testosterone diffusivity in the 1 : 1 v/v ethanol : PBS (water) mixture (D_m^∞) was estimated from the Leffler–Cullinan correlation:[39]

$$ln\left(D_m^\infty\right) = x_w \ln\left(D_w^\infty\right) + x_e \ln\left(D_e^\infty\right) + x_w \ln\left(\frac{\eta_w}{\eta_m}\right) + x_e \ln\left(\frac{\eta_e}{\eta_m}\right) \quad (11)$$

with x_w, x_e designating the mole fractions of water and ethanol in the mixture, D_w^∞ and D_e^∞ the diffusion coefficients of dilute testosterone in water and ethanol (calculated from the Wilke–Chang correlation) and η_e = 1.1 cP and η_m = 2.4 cP are the viscosities of ethanol and the mixtures, respectively, at 25 °C.[40]

Results and discussion

Flow rate

Flow-through system parameters such as receptor cell volume, flow rate, sampling frequency and collector tube volume have been reported to modify the apparent flux[41] and the onset of steady state.[26] The flow rates in the μFPA were set at 4 μL min^{-1} in the silicone membrane experiments and 8 μL min^{-1} in those with skin-OTCs, where higher fluxes were expected. These flow rates maintained receptor sink conditions over the course of the experiment, avoided excessive permeant dilution in the outflow volumes, and allowed for collection volumes smaller than the maximum 96-well plate capacity (<300 μL) and minimal lower limits of detection (LOD). In order to collect the outflow during each time interval in a single well, maximum time intervals of 1 h and 30 min were allowed with receptor flow rates of 4 and 8 μL min^{-1}, respectively. These flow rates determine an outflow volume of 240 μL at these maximum time intervals, which enables LODs of 0.1 μg mL^{-1} for caffeine and salicylic acid, and 0.4 μg mL^{-1} for testosterone. The limits of quantitation (LOQ) are 0.4 μg mL^{-1} and 1.2 μg mL^{-1}, respectively.

Permeation in μFPA *vs.* Franz cell

Permeation through silicone membranes. Fig. 4 shows the receptor cumulative amount profiles of caffeine, salicylic acid and testosterone in the μFPA and in the Franz cells. Mass balance calculations show that recovery of the applied drug in the μFPA is as good as in the Franz cells and within the recommended guidelines of (100 ± 10) % (Table 2). The steady state fluxes (J_{ss}), permeability coefficients (k_p) and lag times (t_{lag}) obtained from the cumulative amount profiles are reported in Table 2. Differences in the mean lag times between the two systems are consistently less than 10 min. The differences in the estimated cumulative amounts and fluxes can be due to variations in the nominal diffusion areas of the two systems; these can be related to manufacturing tolerances for the Franz cell orifice diameter (±0.3 mm) as well as to small deformations of the membranes caused by the clamping mechanisms.[28] The transport of caffeine and salicylic acid in the μFPA and in the Franz cells are essentially identical. Steady state flux and permeability coefficients agree within 10% of their mean values. For testosterone, the μFPA flux and permeability coefficient are 11% lower compared to the Franz cells. This difference is due to testosterone

 This journal is © The Royal Society of Chemistry 2017

Open Access Article. Published on 03 April 2017. Downloaded on 9/22/2024 3:56:12 AM.
This article is licensed under a Creative Commons Attribution 3.0 Unported Licence.

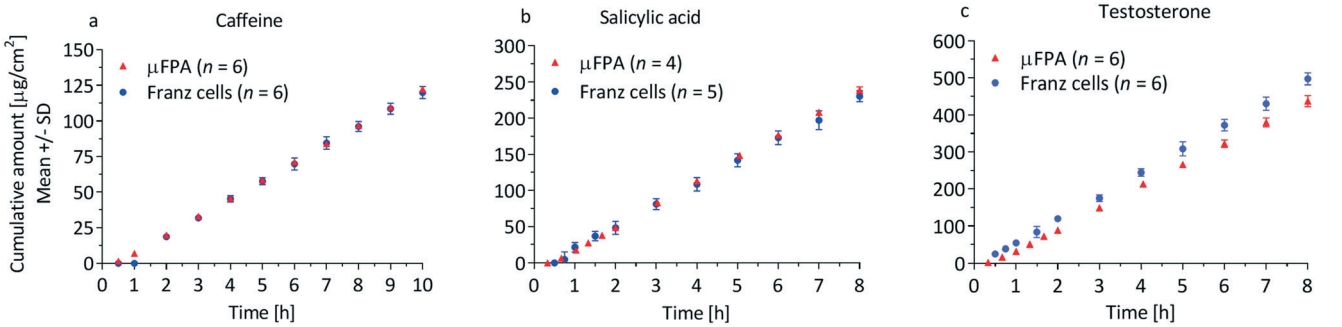

Fig. 4 Cumulative amount profiles of (a) caffeine, (b) salicylic acid and (c) testosterone through silicone membranes in the μFPA and the Franz cells.

Table 2 Steady state flux (J_{ss}), lag time (t_{lag}) and permeability coefficient (k_p) obtained from the cumulative amount profiles in the silicone membrane permeation experiments (data shown as mean ± standard deviation). The mean testosterone J_{ss} and k_p adjusted for accumulation in the μFPA are reported in parentheses

	μFPA	Franz cells
Caffeine	$n = 6$	$n = 6$
J_{ss} [μg cm^{-2}]	13 ± 0.13	13 ± 0.36
t_{lag} [h]	0.43 ± 0.022	0.45 ± 0.072
k_p [10^{-3} cm h^{-1}]	0.93 ± 0.03	0.94 ± 0.01
Permeant recovered [%]	97.1 ± 1.1	100.8 ± 1.3
Salicylic acid	$n = 4$	$n = 5$
J_{ss} [μg cm^{-2}]	32 ± 0.60	30 ± 0.34
t_{lag} [h]	0.43 ± 0.03	0.32 ± 0.11
k_p [10^{-3} cm h^{-1}]	11 ± 0.21	10 ± 0.12
Permeant recovered [%]	99.8 ± 0.8	103.2 ± 2.2
Testosterone	$n = 6$	$n = 6$
J_{ss} [μg cm^{-2}]	57 (62) ± 4.9	64 ± 2.0
t_{lag} [h]	0.36 ± 0.11	0.22 ± 0.16
k_p [10^{-3} cm h^{-1}]	8.2 (8.9) ± 0.70	9.2 ± 0.29
Permeant recovered [%]	98.5 ± 4.5	103.4 ± 1.7

accumulation in the μFPA receptor (Fig. 5a). As verified by numerical simulations, accumulation was significant only in the testosterone experiment. Fig. 5b compares the simulated mass flowing out of the receptor ($M_{out,sim}$) with the mass penetrating into it from the membrane ($M_{m/r,sim}$). At steady state, the ratio between these two mass flows ($M_{out,sim}/M_{m/r,sim}$) stabilizes to a value of 1.09. Multiplication of this accumulation factor to the experimental mean testosterone flux and permeability coefficient yields corrected values of 62 μg (cm^{-2} h^{-1}) and 0.0089 cm h^{-1} for the μFPA, in agreement with the Franz cell results (Table 2). This accumulation factor is confirmed by the testosterone mass recovered from the μFPA receptors at the end of the experiment (~9 μg). This adds ~46 μg cm^{-2} to the total penetrated amount at time 8 h, yielding a final μFPA cumulative amount that more accurately reflects the Franz cell values. The relevant accumulation of testosterone in the μFPA is due to the lower diffusivity of testosterone in the receptor solution. Small volume flow-through cells have been reported to decrease accumulation[28] compared to high volume flow-through cells. In a small volume system such as the μFPA, accumulation can be minimized by increasing the flow rate and the outlet channel size. To demonstrate the possibility to limit accumulation, we increased the μFPA's outlet channel size from 0.3 to 0.75 mm and scaled the receptor chamber height accordingly. Fig. 5c shows good agreement between the testosterone cumulative amounts obtained from the modified μFPA and Franz cells. Differences in the steady state fluxes and permeability coefficients are about 4% (Table 3).

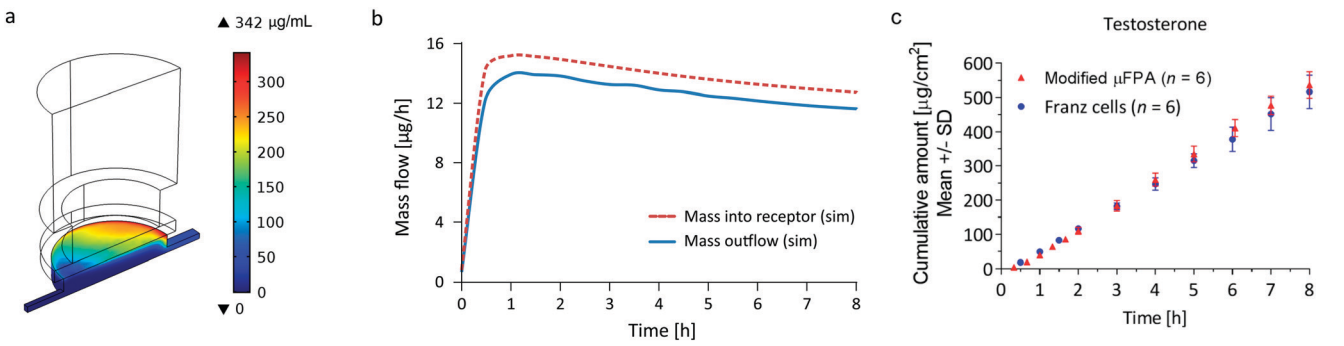

Fig. 5 Simulation results for the determination of testosterone accumulation in the μFPA's receptor chamber. (a) Simulated testosterone concentration in the μFPA: the mass accumulates in the receptor towards the outlet channel. (b) Comparison of the simulated testosterone mass flowing from the membrane into the receptor (dashed line) with the mass flowing out of the outlet channel (continuous line). (c) Cumulative amount profiles of testosterone through silicone membranes in the μFPA modified to eliminate permeant accumulation in the receptor compartment and Franz cells.

Open Access Article. Published on 03 April 2017. Downloaded on 9/22/2024 3:56:12 AM.
This article is licensed under a Creative Commons Attribution 3.0 Unported Licence.

Table 3 Testosterone steady state flux (J_{ss}), lag time (t_{lag}) and permeability coefficient (k_p) obtained from the cumulative amount profiles in the silicone membrane permeation experiments conducted with the μFPA modified to eliminate receptor chamber accumulation (data shown as mean ± standard deviation)

	Modified μFPA (n = 6)	Franz cells (n = 6)
J_{ss} [μg cm^{-2}]	70.4 ± 2.8	68 ± 7.2
t_{lag} [h]	0.28 ± 0.19	0.33 ± 0.16
k_p [10^{-3} cm h^{-1}]	10.2 ± 0.40	9.8 ± 0.10
Permeant recovered [%]	91.4 ± 5.2	101.7 ± 2.1

The precision of the two systems was assessed from the coefficients of variation (CV) of the steady state cumulative amount values. Sources of variations may be related to the manufacturing tolerances for the Franz cell orifice diameter and to small deformations of the clamped membranes. For caffeine and salicylic acid, the steady state cumulative amount CVs range from 1 to 2% in the μFPA, and 3 to 8% in the Franz cells, indicating higher measurement precision in the former (Fig. 4a and b). For testosterone, CVs are 6 to 8% in the unmodified μFPA *vs.* 3 to 6% in the Franz cells (Fig. 4c). The somewhat lower precision in the μFPA's testosterone test is due to cumulative amounts obtained from one of the six permeation chambers. In the comparison of the modified μFPA to Franz cells (Fig. 5c), CVs are 5 to 8% in the μFPA, comparable to the 5 to 10% obtained in the Franz cells.

Khan *et al.* reported high CVs for caffeine (64.9%) and for testosterone (32.3%) permeation through PDMS membranes in Franz cells.[42] Provin *et al.* tested their microfluidic diffusion cell with caffeine through a lipid coated membrane, reporting an average CV of 52.3%.[20] Ng *et al.* achieved a CV of 6% for ibuprofen permeation through PDMS membranes on Franz cells.[43] Bosman *et al.* obtained CVs around 10% in a flow-through cell for transport of [^{3}H] dexetimide through Silastic® membranes.[44] None of these studies reached CVs as low as the ones achieved by our μFPA. Overall, the μFPA enables higher precision when compared directly to the Franz cell or to other systems for permeation testing.

A possible explanation for the lower variability observed in the μFPA is the fact that the whole perfusate is assayed, while in the static Franz cell only samples of the receptor solution are used for quantification of the permeate. Moreover, the higher reproducibility of the geometrical features in the μFPA due to the computer numerical control machining aids minimizing the variability. It is expected that fabrication by injection molding may enhance this effect.

The cumulative amount profiles in Fig. 4 also show that, with the analytical method used in this study, concentrations of the initial permeation time points can be measured only in the μFPA experiments. This higher sensitivity is due to the smaller volumes in which the permeated compounds are diluted. Since the initial permeation typically follows an exponential profile, the μFPA may allow a more accurate estimate of the lag time if the entire experimental cumulative amount curve is fit directly to eqn (3). Consequently the use of the μFPA can also be advantageous for finite dose experiments, for which sharper changes in the flux need to be detected and smaller permeation rates need to be quantified.

Permeation through skin-OTCs. A histological section of the skin-OTC in shown in Fig. 6a. Fig. 6b shows the receptor cumulative amounts of caffeine following permeation through the skin-OTCs. The steady state cumulative amounts in the μFPA are about 20% greater than in the Franz cells. The resulting mean permeability coefficients are 0.051 cm h^{-1} and 0.045 cm h^{-1}, a 13% difference (Table 4). The permeability values suggested an UWL might be affecting transport into the receptor solutions.[8] The UWL experiments confirm this, with mean diffusive resistances of 2.54 and 6.13 h cm^{-1} estimated in the μFPA and the Franz cells, respectively (Fig. 6c). These are due to approximately 0.062 and 0.15 cm-thick UWLs, likely forming mainly in the unstirred donor compartments of the μFPA and Franz cells. Factoring in the effect of the UWLs, the mean μFPA and Franz cell permeability coefficients increase to 0.062 and 0.059 cm h^{-1}, reducing the difference to 6.1% (Table 4). The presence of a UWL and its impact in an *in vitro* transport study depend on the diffusion cell's design, the permeant, the membrane, and the solvent (receptor solution) under consideration.[8,45,46] For a given membrane in contact with an aqueous solution, a greater

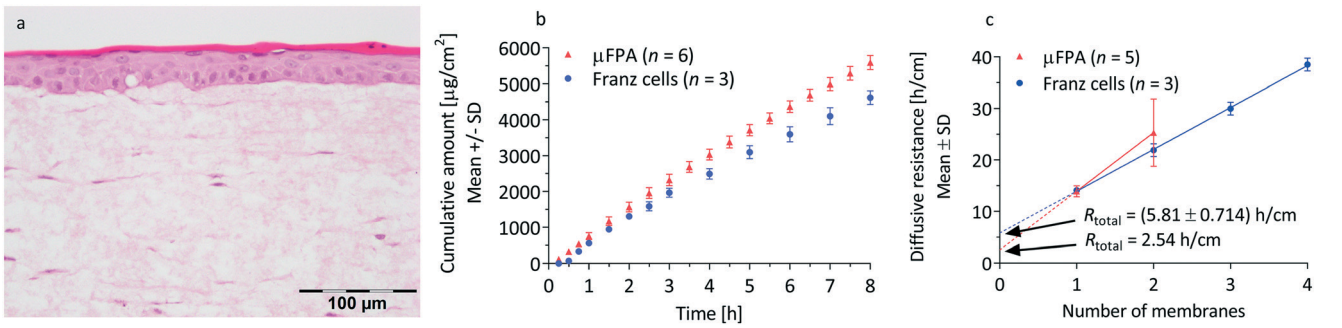

Fig. 6 (a) Representative hematoxylin and eosin-stained section of the full-thickness skin organotypic culture (skin-OTC) used in the caffeine permeation experiment. (b) Cumulative amount profiles of caffeine through the skin-OTC in the μFPA *vs.* Franz cells. (c) Total resistances to caffeine diffusion in the unstirred water layer (UWL) experiments.

 This journal is © The Royal Society of Chemistry 2017

Open Access Article. Published on 03 April 2017. Downloaded on 9/22/2024 3:56:12 AM.
This article is licensed under a Creative Commons Attribution 3.0 Unported Licence.

Table 4 Steady state flux (J_{ss}), lag time (t_{lag}) and permeability coefficient (k_p) obtained from the cumulative amount profiles of caffeine through skin-OTC in the μFPA and in the Franz cells (data shown as mean ± standard deviation). The mean μFPA and Franz cell J_{ss} and k_p corrected for their respective UWLs are reported in parentheses

	μFPA (n = 6)	Franz cells (n = 3)
J_{ss} [μg cm^{-2}]	670 (788) ± 23	600 (836) ± 26
t_{lag} [h]	~0	~0
k_p [10^{-3} cm h^{-1}]	51 (59) ± 1.7	45 (62) ± 1.9
Permeant recovered [%]	95.6 ± 1.8	90.9 ± 2.1

fraction of the diffusional resistance can be attributed to a UWL for more lipophilic permeants.[8]

The CV of the cumulative amounts in the steady state regime stabilizes around 3% in the μFPA experiments, and around 5% in the Franz cells, indicating higher measurement precision in the former. These CV values are calculated from the combined results of both μFPAs and of both skin tissues used in this test. The μFPA's inter-chip and inter-OTC variability for caffeine permeating through the skin-OTC is very low. Similarly, the bulk materials of the chip (PC and PMMA) did not affect the reproducibility or the precision, with steady state cumulative amounts in the PC and PMMA chips differing by less than 4% and the derived flux and permeability coefficients by less than 2%.

Conclusions and outlook

In this study, we presented and validated a microfluidic platform for improved, cost-effective *in vitro* skin permeation testing. This μFPA yields comparable or lower variability in the results, allows quantitation of lower permeation rates and reduces the problem of UWLs. In contrast to other miniaturization attempts,[9–11] the μFPA was developed following the principles of design for manufacturing, with a standard format size and a body made of a thermoplastic material; thus it is suitable for mass production techniques. The possibility of using PC, PMMA or cyclic olefin copolymer for the bulk of the μFPA overcomes issues related to adsorption of lipophilic compounds usually associated with PDMS. The six-chamber version of the μFPA described here allows for an adequate number of replicates as recommended by OECD guidelines for skin absorption[30] and by the FDA's Guidance for Industry for *in vitro* release testing of semisolid dosage form.[47] The throughput can be easily increased by using more μFPAs in parallel and is only limited by the number of available perfusion channels in the pumps. The design of the μFPA can also be modified to integrate more permeation chambers, further reducing the cost of a replicate. In addition, maintenance of the skin surface temperature at 32 °C can be achieved by either placing the μFPA on a hotplate or pre-heating the receptor solution.

The cost of the experiment is significantly reduced as the μFPA requires ten-fold smaller skin tissues and lower amounts of tested drugs compared to Franz diffusion cells. Six glass-made Franz diffusion cells with large fabrication tolerances are replaced by an equivalent multi-chamber disposable plastic chip. As the proposed analytical method only requires a microplate reader, the μFPA is a convenient option for those laboratories where expensive and sophisticated instrumentation such as high-performance liquid chromatography or mass spectroscopy is not available.

Because of the simplicity of the μFPA, the fraction collection process and the procedural steps required for a valid mass balance can be automated by means of a downstream collecting system and an upstream fluidic control system, respectively. The downstream collecting system will automatically slide the 96-well plates placed under the chip at predetermined time intervals, enabling long-term experiments with minimal manual operations. The upstream fluidic control system should be programmable and its operation coordinated with the downstream collecting system. For finite dose protocols[48] involving liquid or gaseous substances, exposure to the skin could be automated in the μFPA by integrating microfluidics on the donor side.

The validation of this μFPA is a critical step towards the development of a skin-on-chip device for reliable, standardized and high-throughput skin permeation and toxicity assays.

Acknowledgements

This research was financially supported by Singapore A*STAR's Joint Council Office, grant no. 1334 K00081. We thank Dr. Bhimsen Rout (Institute of Medical Biology, A*STAR) and Matthew A. Miller (James L. Winkle College of Pharmacy, University of Cincinnati) for helpful discussions.

Notes and references

1 S. Wiedersberg and R. H. Guy, *J. Controlled Release*, 2014, **190**, 150–156.
2 D. Karadzovska and J. E. Riviere, *Eur. J. Pharm. Sci.*, 2013, **50**, 569–576.
3 H. E. Buist, G. Schaafsma and J. J. M. van de Sandt, *Regul. Toxicol. Pharmacol.*, 2009, **54**, 221–228.
4 M. A. Ngo, M. O'Malley and H. I. Maibach, *J. Appl. Toxicol.*, 2010, **30**, 91–114.
5 C. J. Weschler and W. W. Nazaroff, *Indoor Air*, 2012, **22**, 356–377.
6 S. Schreiber, A. Mahmoud, A. Vuia, M. Rübbelke, E. Schmidt, M. Schaller, H. Kandarova, A. Haberland, U. Schäfer and U. Bock, *Toxicol. In Vitro*, 2005, **19**, 813–822.
7 M. R. Prausnitz, S. Mitragotri and R. Langer, *Nat. Rev. Drug Discovery*, 2004, **3**, 115–124.
8 M. A. Miller and G. Kasting, *Pharm. Dev. Technol.*, 2012, **17**, 705–711.
9 P. E. Nielsen and A. Avdeef, *Eur. J. Pharm. Sci.*, 2004, **22**, 33–41.
10 S. N. Bhatia and D. E. Ingber, *Nature*, 2014, **201**, 4.

Open Access Article. Published on 03 April 2017. Downloaded on 9/22/2024 3:56:12 AM.
This article is licensed under a Creative Commons Attribution 3.0 Unported Licence.

11 Q. Ramadan and F. C. W. Ting, *Lab Chip*, 2016, **16**, 1899–1908.
12 B. Ataç, I. Wagner, R. Horland, R. Lauster, U. Marx, A. G. Tonevitsky, R. P. Azar and G. Lindner, *Lab Chip*, 2013, **13**, 3555–3561.
13 I. Maschmeyer, A. K. Lorenz, K. Schimek, T. Hasenberg, A. P. Ramme, J. Hübner, M. Lindner, C. Drewell, S. Bauer and A. Thomas, *Lab Chip*, 2015, **15**, 2688–2699.
14 I. Wagner, E.-M. Materne, S. Brincker, U. Süßbier, C. Frädrich, M. Busek, F. Sonntag, D. A. Sakharov, E. V. Trushkin and A. G. Tonevitsky, *Lab Chip*, 2013, **13**, 3538–3547.
15 L. Hou, J. Hagen, X. Wang, I. Papautsky, R. Naik, N. Kelley-Loughnane and J. Heikenfeld, *Lab Chip*, 2013, **13**, 1868–1875.
16 R. Peng, Z. Sonner, A. Hauke, E. Wilder, J. Kasting, T. Gaillard, D. Swaille, F. Sherman, X. Mao and J. Hagen, *Lab Chip*, 2016, **16**, 4415–4423.
17 Z. Sonner, E. Wilder, J. Heikenfeld, G. Kasting, F. Beyette, D. Swaile, F. Sherman, J. Joyce, J. Hagen and N. Kelley-Loughnane, *Biomicrofluidics*, 2015, **9**, 031301.
18 C. S. Mah, J. Singh Kochhar, P. S. Ong and L. Kang, *Int. J. Pharm.*, 2013, **441**, 433–440.
19 H. E. Abaci, K. Gledhill, Z. Guo, A. M. Christiano and M. L. Shuler, *Lab Chip*, 2015, **15**, 882–888.
20 C. Provin, A. Nicolas, S. Grégoire and T. Fujii, *Pharm. Res.*, 2015, **32**, 2704–2712.
21 N. Li, M. Schwartz and C. Ionescu-Zanetti, *J. Biomol. Screening*, 2009, **14**, 194–202.
22 K. Ren, J. Zhou and H. Wu, *Acc. Chem. Res.*, 2013, **46**, 2396–2406.
23 M. W. Toepke and D. J. Beebe, *Lab Chip*, 2006, **6**, 1484–1486.
24 P. M. van Midwoud, A. Janse, M. T. Merema, G. M. M. Groothuis and E. Verpoorte, *Anal. Chem.*, 2012, **84**, 3938–3944.
25 R. Chilcott, N. Barai, A. Beezer, S. Brain, M. Brown, A. Bunge, S. Burgess, S. Cross, C. Dalton and M. Dias, *J. Pharm. Sci.*, 2005, **94**, 632–638.
26 M. Córdoba-Díaz, M. Nova, B. Elorza, D. Córdoba-Díaz, J. Chantres and M. Córdoba-Borrego, *J. Controlled Release*, 2000, **69**, 357–367.
27 S.-F. Ng, J. J. Rouse, F. D. Sanderson, V. Meidan and G. M. Eccleston, *AAPS PharmSciTech*, 2010, **11**, 1432–1441.
28 W. G. Reifenrath, B. Lee, D. R. Wilson and T. S. Spencer, *J. Pharm. Sci.*, 1994, **83**, 1229–1233.
29 L. Bartosova and J. Bajgar, *Curr. Med. Chem.*, 2012, **19**, 4671–4677.
30 OECD, *Test No. 428. OECD Guideline for Testing of Chemicals: Skin Absorption: In Vitro Method*, OECD Publishing, 2004.
31 J. J. M. van de Sandt, J. A. van Burgsteden, S. Cage, P. L. Carmichael, I. Dick, S. Kenyon, G. Korinth, F. Larese, J. C. Limasset, W. J. M. Maas, L. Montomoli, J. B. Nielsen, J. P. Payan, E. Robinson, P. Sartorelli, K. H. Schaller, S. C. Wilkinson and F. M. Williams, *Regul. Toxicol. Pharmacol.*, 2004, **39**, 271–281.
32 R. G. Wu, Z. P. Wang, H. Xia, W. Fan, W. C. Wang, M. K. Teo, J. Salmon and J. O'Halloran, *Lab on a chip Asia*, Singapore, November, 2014.
33 M. A. Dickson, W. C. Hahn, Y. Ino, V. Ronfard, J. Y. Wu, R. A. Weinberg, D. N. Louis, F. P. Li and J. G. Rheinwald, *Mol. Cell. Biol.*, 2000, **20**, 1436–1447.
34 P. P. C. Toh, M. Bigliardi-Qi, A. M. Y. Yap, G. Sriram and P. Bigliardi, *Exp. Dermatol.*, 2016, **25**, 1002–1005.
35 J. Krüse, D. Golden, S. Wilkinson, F. Williams, S. Kezic and J. Corish, *J. Pharm. Sci.*, 2007, **96**, 682–703.
36 C. Wilke and P. Chang, *AIChE J.*, 1955, **1**, 264–270.
37 E. Baum, *Chemical Property Estimation: Theory and Application*, Lewis Publishers, 1997.
38 D. J. Harrison and K. Knutson, *Pharm. Res.*, 1995, **12**, 2003–2011.
39 A. Safi, C. Nicolas, E. Neau and J. Escandell, *J. Chem. Eng. Data*, 2010, **55**, 5449–5452.
40 I. S. Khattab, F. Bandarkar, M. A. A. Fakhree and A. Jouyban, *Korean J. Chem. Eng.*, 2012, **29**, 812–817.
41 J. Sclafani, J. Nightingale, P. Liu and T. Kurihara-Bergstrom, *Pharm. Res.*, 1993, **10**, 1521–1526.
42 G. M. Khan, Y. Frum, O. Sarheed, G. M. Eccleston and V. M. Meidan, *Int. J. Pharm.*, 2005, **303**, 81–87.
43 S.-F. Ng, J. Rouse, D. Sanderson and G. Eccleston, *Pharmaceutics*, 2010, **2**, 209–223.
44 I. J. Bosman, S. R. Avegaart, A. L. Lawant, K. Ensing and R. A. de Zeeuw, *J. Pharm. Biomed. Anal.*, 1998, **17**, 493–499.
45 W. J. Addicks, G. L. Flynn and N. Weiner, *Pharm. Res.*, 1987, **4**, 337–341.
46 T. Korjamo, A. T. Heikkinen and J. Mönkkönen, *J. Pharm. Sci.*, 2009, **98**, 4469–4479.
47 SUPAC-SS, *Guidance for industry: nonsterile semisolid dosage forms, scale-up and post approval changes: chemistry, manufacturing and controls; in vitro release testing and in vivo bioequivalence documentation*, 1997.
48 Y. Dancik, P. L. Bigliardi and M. Bigliardi-Qi, *Reprod. Toxicol.*, 2015, **58**, 252–281.

This journal is © The Royal Society of Chemistry 2017